Available online at www.sciencedirect.com
ScienceDirect
Journal of Solid State Chemistry 180 (2007) 2485–2492
JOURNAL OF SOLID STATE CHEMISTRY
www.elsevier.com/locate/jssc

# Synthesis and $CO_2$ capture evaluation of $Li_{2-x}K_xZrO_3$ solid solutions and crystal structure of a new lithium–potassium zirconate phase

Mayra Y. Veliz-Enriquez[a], Gonzalo Gonzalez[b], Heriberto Pfeiffer[b,*]

[a]*Facultad de Ingeniería Química, Benemérita Universidad Autónoma de Puebla, Puebla, Mexico*
[b]*Instituto de Investigaciones en Materiales, Universidad Nacional Autónoma de México, Circuito exterior s/n Ciudad Universitaria, Del. Coyoacán, CP 04510, México DF, Mexico*

Received 27 February 2007; received in revised form 18 May 2007; accepted 24 June 2007
Available online 3 July 2007

**Abstract**

Solid solutions of lithium and potassium metazirconates $Li_{2-x}K_xZrO_3$ (where, $0 \leqslant x \leqslant 2$) were prepared by coprecipitation. Samples were characterized by powder X-ray diffraction, scanning electron microscopy, and thermogravimetric analyses. Results showed that the solubility limits of potassium into $Li_2ZrO_3$ is $x = 0.2$. Furthermore, at higher potassium concentrations, a new phase was synthesized, $Li_{2.27}K_{1.19}Zr_{2.16}O_{6.05}$. For structural studies of this new phase, XRD data were analyzed by Rietveld refinements. Additionally, at high potassium concentrations different phases of $ZrO_2$ were found, as potassium tends to sublimate. On the other hand, lithium–potassium metazirconate solid solutions, $Li_{2-x}K_xZrO_3$, were tested as $CO_2$ captors. Thermal analyses into a $CO_2$ flux showed that $Li_{2-x}K_xZr_2O_3$ solid solutions present a better $CO_2$ absorption than $Li_2ZrO_3$ pure. The differences observed in the $CO_2$ sorption processes were explained with thermodynamic data.


*Keywords:* $CO_2$ capture; Rietveld refinement; X-ray diffraction; Zirconate

## 1. Introduction

Lithium ceramics are of research interest because of their different technological applications. For example, there has been research in recent years on their application as electronic devices in batteries, as breeder materials for nuclear fusion reactors, and in low thermal expansion glass–ceramics [1–4]. Additionally, in the last nine years lithium ceramics have been studied as carbon dioxide ($CO_2$) captors [5–10].

Due to the global warming, the capture, elimination and storage of $CO_2$ have becoming a very important issue around the world. In this way, different kinds of materials have been proposed as $CO_2$ captors, such as zeolites, perovskites, soda lime, hydrotalcites and polymeric membranes, among others [11–14]. However, all these materials present one or more disadvantages. Hence, new materials for the $CO_2$ capture must have very specific properties: (1) high selectivity and sorption capacity for $CO_2$ at elevated temperatures, (2) adequate absorption/desorption kinetics for $CO_2$, (3) good cyclability for the absorption/desorption process and (4) good hydrothermal and mechanical properties [7]. In this sense, several lithium and sodium ceramics seem to present good properties for the $CO_2$ capture. Among these ceramics, it has been published that lithium–sodium zirconates solid solutions ($Li_{2-x}Na_xZrO_3$) present better $CO_2$ properties than pure lithium or sodium zirconates [15,16]. Moreover, it has been published that $Li_2ZrO_3$ doped with very small quantities of potassium enhances its $CO_2$ capture capacity [17]. Hence, mixed compounds $Li_2ZrO_3$–$K_2ZrO_3$ could present similar behaviors in $CO_2$ sorption than that observed for the $Li_{2-x}Na_xZrO_3$ solid solutions. In addition, there is not any study of these oxide solid solutions, $Li_{2-x}K_xZrO_3$. Only in 1996, Mather and coworkers [18] reported the following crystalline structure $Li_{1.8}K_{0.9}Mg_{0.75}Zr_{2.25}O_{6.6}$, which may be associated the $Li_{2-x}K_xZrO_3$ compounds, although it contains magnesium. Therefore, the aim of this paper was to study the synthesis of such compounds,

*Corresponding author. Fax: +52 55 5616 1371.
*E-mail address:* pfeiffer@iim.unam.mx (H. Pfeiffer).

0022-4596/$ - see front matter © 2007 Elsevier Inc. All rights reserved.
doi:10.1016/j.jssc.2007.06.023

characterize them systematically, and to study their $CO_2$ retention capacities.

## 2. Experimental section

Zirconates were prepared by co-precipitation method. Stoichiometric amounts of lithium carbonate ($Li_2CO_3$), potassium carbonate ($K_2CO_3$) and zirconium acetate ($Zr(OCH_3)_4$) were mixed and dissolved, to obtain the nominal solid solution $Li_{2-x}K_xZrO_3$, where $x$ was equal to 0, 0.1, 0.2, 0.3, 0.4, 0.6, 1.0, 1.4, 1.6 and 1.8. Actually, these nominal values were used to label the samples, for example $Li_{1.8}Na_{0.2}ZrO_3$. Each solution was stirred in water for 2 h. Then, the solution was heated at 70 °C until the precipitate dried. Finally, the powders were heat treated at 900 °C for 4 h.

The samples were characterized by X-ray diffraction (XRD), scanning electron microscopy (SEM) and thermogravimetric analysis (TGA). To obtain the XRD patterns, it was used a $\theta-2\theta$ diffractometer (BRUKER axs, D8 Advance), using Cu$K\alpha$ radiation, $\lambda = 1.54056$ Å, at 35 kV and 30 mA. The relative percentages of the various compounds, identified by the corresponding JCPDS files (Joint Committee on Powder Diffraction Standards), were estimated from the total area under the most intense diffraction peak for each phase. The estimated experimental error was $\pm 3\%$. For determination of lattice parameters and for structural studies of the new phase, the scanned range was only performed where the main peaks of these materials are presented (10–80° $2\theta$), with a step of 0.02° $2\theta$ and 10 s/step. For structural refinements, from X-ray powder diffraction data, the FullProf-Suite program was used as Rietveld software [19]. The background was approximated by a linear interpolation of 80 data points. The profile function, which was used to describe the peak shape, was a Thompson–Cox–Hastings pseudo-Voigt function. Instrumental profiles, based on $LaB_6$ standard, were incorporated to the refinement.

A scanning electron microscope (SEM), Stereoscan 440 Cambridge, was used to determine the particle size and morphology of the samples. In order to avoid the lack of conductivity of the samples, they were previously covered with gold.

At last but not least, $CO_2$ sorption analyses were performed on the different samples in a 2950 Thermogravimetric Analyzer, TA Instruments. Samples were heat treated with a heating rate of 5 °C min$^{-1}$ from room temperature to 1000 °C, into a $CO_2$ flux. Finally, isothermals experiments were perform in the same equipment at 550 °C under a $CO_2$ atmosphere.

## 3. Results and discussion

### 3.1. Composition and structure

$Li_2ZrO_3$, which has a monoclinic structure, and $Li_{2-x}K_xZrO_3$ solid solutions were obtained using different Li:K molar ratios. Some of these diffractograms are shown in Fig. 1. Samples with $x = 0$ and 0.2 only showed the presence of $Li_2ZrO_3$. However, if the $x$ value was increased to 0.3, a second phase was also found. This new phase was identified as an isostructural compound of the $Li_{1.8}K_{0.9}Mg_{0.75}Zr_{2.25}O_{6.6}$ phase previously reported by Mather and coworkers [18]. Of course, in this sample, there is not magnesium available. Therefore, one of the alkaline elements could occupy these positions. A chemical elemental analysis was performed in order to know the composition of the sample. Results indicate that the chemical formula is equal to $Li_{2.27}K_{1.19}Zr_{2.16}O_{6.05}$. Nevertheless, it has to be pointed out that the sample was not pure. A further crystallographic analysis, of this compound, was performed (see below, Section 3.2).

Coming back to the solid solution compositions, as the $x$ value increased, mixtures of $Li_2ZrO_3$ and the isostructural phase were observed. Nevertheless, the $Li_2ZrO_3$ disappeared when $x$ reached 1.0. It was related to the detection of different $ZrO_2$ phases, tetragonal and monoclinic. Finally, at higher $x$ values a different phase appeared, $K_2Zr_3O_7$. These results are summarized in Fig. 2. One result comes out with this figure, the presence of $ZrO_2$ phase. The presence of

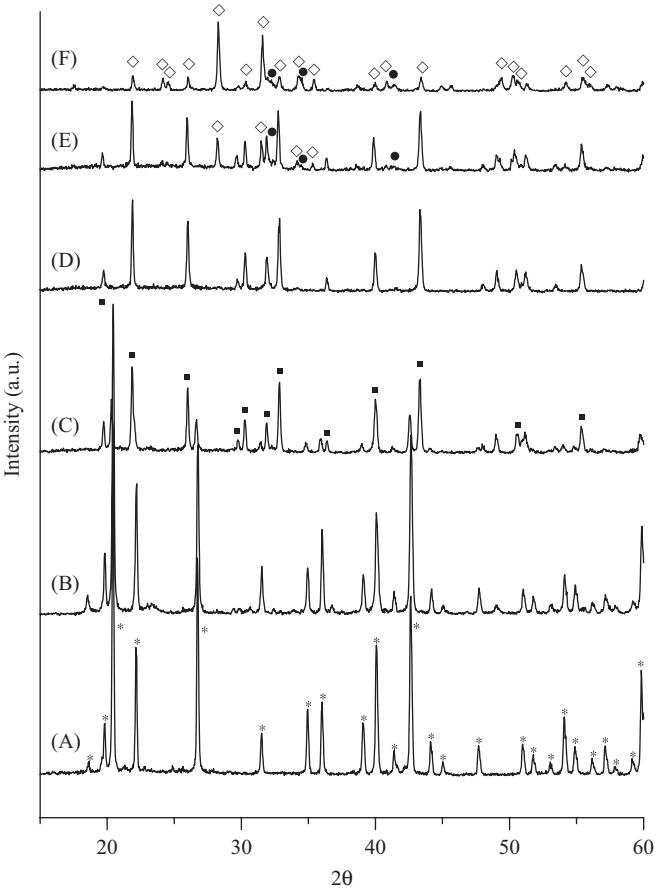


Fig. 1. XRD patterns of the $Li_{2-x}K_xZrO_3$ samples heat treated for 4 h at 900 °C. Capital letters indicate to different value of $x$ on $Li_{2-x}K_xZrO_3$ nominal composition: (A) $x = 0.0$, (B) $x = 0.2$, (C) $x = 0.3$, (D) $x = 1.0$, (E) $x = 1.4$ and (F) $x = 1.8$. The label peaks correspond to (*) $Li_2ZrO_3$, (■) $Li_{2.27}K_{1.19}Zr_{2.16}O_{6.05}$, (●) $K_2Zr_3O_7$ and (◇) $ZrO_2$.

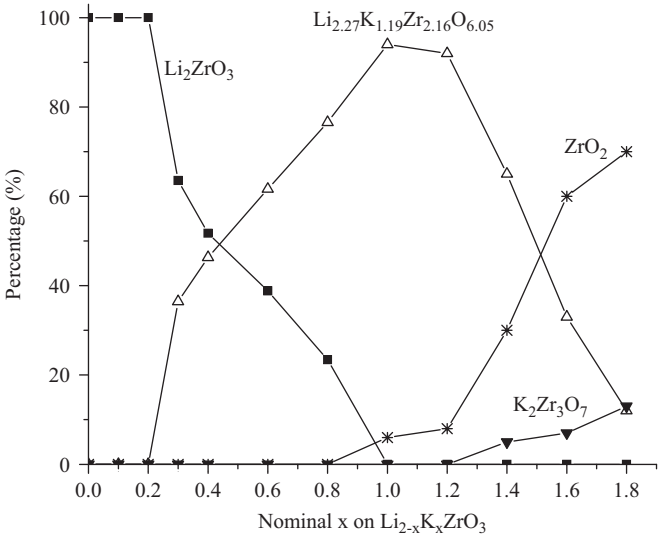


Fig. 2. Percentage of the different phases detected by XRD, as a function of the $x$ value on $Li_{2-x}K_xZrO_3$. The $ZrO_2$ percentage plotted corresponds to the sum of the tetragonal and the monoclinic phases.

$ZrO_2$ and the poor quantities of $K_2Zr_3O_7$ detected at $x$ values higher than 1.2, strongly hint that potassium is being lost in some way. It has been reported that potassium zirconates are not very stable; $K_2ZrO_3$, $K_2Zr_2O_5$ and $K_2Zr_3O_7$ decompose at 570, 720 and 750 °C. In all cases, some potassium is sublimated and the potassium residual stay as dopant into the zirconium oxide [20]. Perhaps, in this case, most of the potassium sublimes due to the high temperature used during the thermal treatments (900 °C). This kind of effect has been observed for other alkaline ceramics, specifically for lithium and sodium ceramics, where the alkaline element sublimes as oxide, at higher temperatures than 700 °C [7,21].

The results clearly show that the solubility limit of potassium into $Li_2ZrO_3$ is equal to 0.2, producing the following nominal formula, $Li_{1.8}K_{0.2}ZrO_3$. However, it cannot be conclusive, due to the high tendency of potassium to sublime. Nevertheless, the results do confirm that most of the potassium atoms are diffusing into the $Li_2ZrO_3$ structure, because the ordered inclusion of potassium expanded the crystalline structure. The cell parameters changed from $a = 5.3454$ Å, $b = 8.8679$ Å, $c = 5.3870$ Å and $\beta = 112.8535°$ to $a = 5.4031$ Å, $b = 8.9421$ Å, $c = 5.403$ Å and $\beta = 112.7741°$ ($Li_{1.8}K_{0.2}ZrO_3$). Such a difference may be simply attributed to the difference in atomic radii of lithium and potassium atoms, 2.05 and 2.77 Å, respectively [22].

### 3.2. Rietveld analysis of the new phase $Li_{2.27}K_{1.19}Zr_{2.16}O_{6.05}$

As it was mentioned previously, a new phase was detected during the synthesis of $Li_{2-x}K_xZrO_3$ solid solutions, but the powders could not be obtained pure despite it was synthesized several times and cleaned with different organic and inorganic solutions. The high reactivity of this material did not let it. Therefore, this sample was used to perform the Rietveld adjustments and different structures were tested varying the lithium and potassium relationship, taking as starting point the isostructural phase reported by Mather and coworkers [18]. In this first case, when magnesium is just substituted by lithium and potassium atoms, the theoretical formula calculated was $Li_{3.75}K_{0.9}Zr_{2.25}O_{6.5}$. This formula did not adjust to the experimental composition obtained by elemental analysis. While there is a 65.2% of lithium excess, the potassium quantity has been diminished on 24.4%. The zirconium and oxygen variations were not so large, 4.2% and 7.4%, respectively. These differences could be explained by two different factors; the low scattering factor of lithium, and the presence of other phases on the sample, containing potassium. Actually, if the occupancy of lithium was not fixed, it could be refined up to 0.6 of occupancy, without changing the Rietveld analysis significantly (data not shown). In this case (occ = 0.6), the lithium excess would be reduced up to 29.9%. Then, Rietveld method sensibility showed to be poor in respect to lithium occupancy and therefore it cannot be determined accurately. On the other hand, when potassium atoms were increased into the theoretical formula, the $R_{bragg}$ increased from 3.74 (using the isostructural initial values), up to 8.68 when lithium was interchanged partially with potassium. After those results, although there should be a combination of lithium and potassium into the structure, some of the potassium detected by the elemental analysis must be present into impurities and not into the phase refined. Based on these results, it was decided to present the Rietveld refinement with better lithium adjusts, 29.9% in excess.

Rietveld refinement results, for this phase, are shown in Fig. 3. The calculations were performed taking as primary data the structure parameters reported previously for the isostructural $Li_{1.8}K_{0.9}Mg_{0.75}Zr_{2.25}O_{6.6}$ compound [18]. In this case, magnesium atoms were switched to lithium and

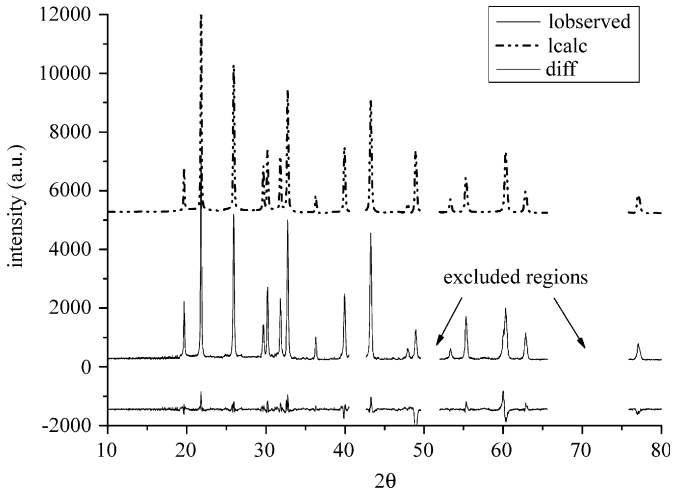


Fig. 3. Calculated (A), experimental (B) and difference (C) X-ray diffraction patterns of the $Li_{2.27}K_{1.19}Zr_{2.16}O_{6.05}$ tetragonal new phase.

potassium atoms, according to the elemental composition previously mentioned. The excluded regions correspond to $ZrO_2$ phase observed on the sample. Excluding the background selected data points, only a few parameters were needed to obtain a good refinement of the compound. Tables 1 and 2 summarize the refined parameters, and the atomic positions of the observed peaks. Among the different results obtained, the $R_{wp}$ value has to be explained. This value could be considered high, but it has to be taken into account the presence of other phases, which were not refined, increasing the $R_{wp}$ value consequently.

Most atoms occupied special positions into the space group, and only $z$ coordinate needed to be refined. These corrections implied a slightly deformation over the $c$-axis (Fig. 4). In this structure, the lithium atoms are located on different positions. While some lithium atoms are hexa-coordinated, Li(1), other lithium atoms are lonely penta-coordinated, Li(2) (Fig. 4-B). The $LiO_6$ polyhedra are distorted along the $c$-axis. On the other hand, the $LiO_5$ polyhedra do not present this kind of distortion. This effect may be attributed to Coulombic repulsion energies associated with the proximity of lithium and potassium atoms. Additionally, Li–O distances on $LiO_5$ and $LiO_6$ varied mainly over the $c$-axis, as it could be expected, it increased 7.88% on $LiO_5$ and 11.6% on $LiO_6$. On the contrary, the Li–O distance only changed 2.2% on the $ab$ plane. Nevertheless, isostructural phase results indicated that $LiO_5$ polyhedra are not totally occupied; its occupancy was established as 87.5%. However, as lithium atoms have a very low scattering factor, when a significant variation was set on this occupancy, results were almost not modified (data not shown). Then, it cannot be concluded that these sites are totally occupied or not.

Zirconium atoms environment leads to two different $ZrO_6$ octahedrons, forming layers at three different sites over the $c$-axis of the cell, $Zr(1)O_6$ polyhedra at the top and bottom and $Zr(2)O_6$ polyhedra on the middle of the cell. Fig. 5 shows the Zr(1) and Zr(2) environments

Table 1
Rietveld refinement parameters of lithium potassium zirconate

| | |
|---|---|
| Tetragonal cell (nm) | $a = 0.41822(8)$, $c = 1.80540(8)$ |
| Space group | I 4/m m m (139) |
| Formula per cell | $Z = 2$ |
| Volume ($nm^3$) | 0.3158 |
| $R_{wp}$ | 24.5 |
| Calculate density ($gr/cm^3$) | 3.808 |
| Refined pattern (2θ, range) | 10–80 |
| Step scan increment (2θ) | 0.02 |
| Wavelength (nm) | 0.154053, 0.154431 |
| No. of points | 3501 |

$R_F = 100\sum_{i=1}^{i=n}\left(I_i^{obs\,1/2} - I_i^{calc\,1/2}\right)/\sum_{i=1}^{i=n} I_i^{obs\,1/2} = 2.03$,
$\chi^2(\text{Goodness of fit}) = (R_{wp}/R_e)^2 = 3.1$,
where $R_{wp} = 100\left(\sum_{i=1}^{i=n} w_i\left(y_i^{obs} - y_i^{calc}\right)^2/\sum_{i=1}^{i=n} w_i y_i^{obs\,2}\right)^{1/2}$
$R_e = 100\left[(N-P+C)/\left(\sum_{i=1}^{i=n} w_i y_i^{obs\,2}\right)\right]^{1/2}$.

Table 2
Atomic positions and occupancies parameters for $Li_{2.27}K_{1.19}Zr_{2.16}O_{6.05}$ tetragonal phase

| Atom | Site | $x/a$ | $y/b$ | $z/c$ | occ |
|---|---|---|---|---|---|
| K(1) | 2b | 0 | 0 | 0.5 | 0.9 |
| Li(1) | 4e | 0 | 0 | 0.34275 | 0.6 |
| Li(2) | 4d | 0 | 0.5 | 0.25 | 0.875 |
| Zr(1) | 4e | 0 | 0 | 0.11246 | 1 |
| Zr(2) | 4d | 0 | 0.5 | 0.25 | 0.125 |
| O(1) | 8g | 0 | 0.5 | 0.125 | 0.93 |
| O(2) | 4e | 0 | 0 | 0.23424 | 0.89 |
| O(3) | 2a | 0 | 0 | 0 | 1 |

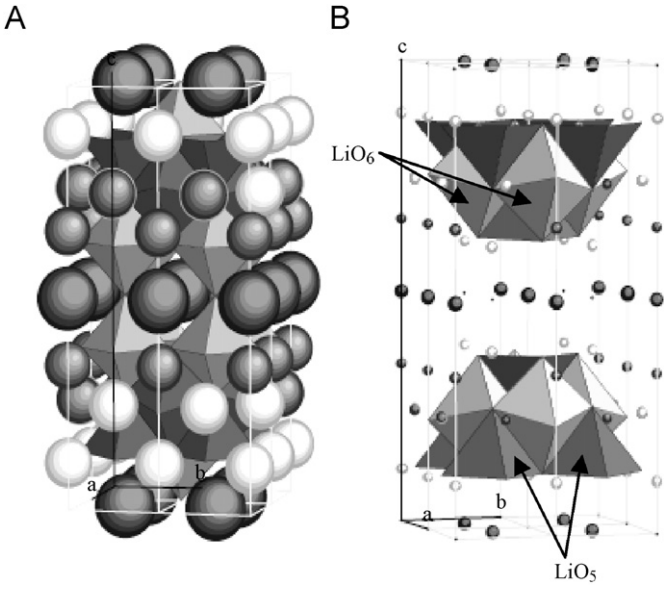


Fig. 4. Crystal structure of $Li_{2.27}K_{1.19}Zr_{2.16}O_{6.05}$ (A) and image showing only the lithium polyhedra: $LiO_5$ and $LiO_6$ (B).

and the modifications observed for the new phase ($Li_{2.27}K_{1.19}Zr_{2.16}O_{6.05}$), in comparison with the isostructural $Li_{1.8}K_{0.9}Mg_{0.75}Zr_{2.25}O_{6.6}$ phase, previously reported. Although, the distance and angle differences, between the two structures, show a global lattice deformation, the higher distortions are present on the $Zr(1)O_6$ polyhedra, and specifically it is produced over the $c$-axis. In other words, the higher distortion is produced on the Zr(1)–O(2) bonds (see Fig. 5). It can be explained by the O(2) first neighbors. In fact, these oxygen atoms are part of the $LiO_6$ polyhedra, which are the polyhedra where magnesium atoms are located on the isostructural phase. Then, the interchange of magnesium atoms by lithium atoms can explain the distortion observed on these parts of the structure, due to the differences on the atomic radii.

### 3.3. Morphology

Different samples were studied by SEM, and the grain size was measured using standard procedures. Micrographs

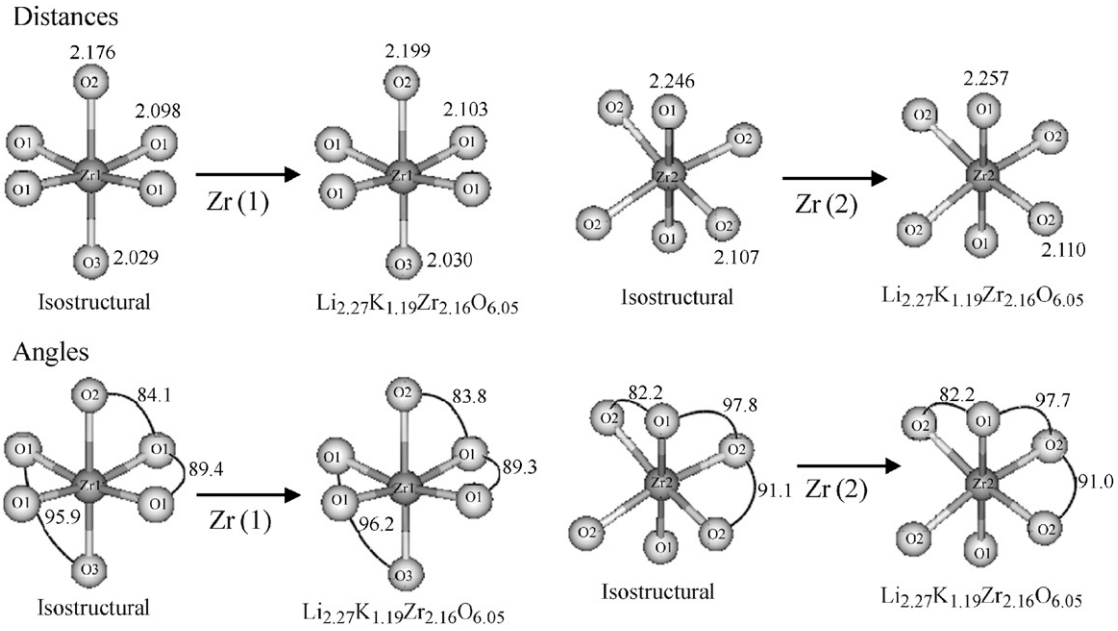


Fig. 5. Deformation of $ZrO_6$ coordination polyhedra. Comparison between the new $Li_{2.27}K_{1.19}Zr_{2.16}O_{6.05}$ phase and the isostructural $Li_{1.8}K_{0.9}Mg_{0.75}Zr_{2.25}O_{6.6}$ compound.

of the lithium zirconate showed the following morphology. The sample showed polyhedral particles with a particle size between 2 and 5 μm, forming agglomerates (Fig. 6A). This kind of morphology corresponds well with the high temperature used during the thermal treatment.

On the contrary, the morphological characteristics of the $Li_{1.8}K_{0.2}ZrO_3$ sample, which is the limit of the solid solution, were slightly different. First, the particle size decreased to less than 1 μm, but the particles seem to agglomerate in particles of more than 20 μm, (Fig. 6B). It seems that the presence of potassium is inhibiting the growth of the particles. As $Li_{1.8}K_{0.2}ZrO_3$ particles are smaller than those of $Li_2ZrO_3$, the surface area should be higher on the second sample. Therefore, this effect may favor the $CO_2$ sorption.

The morphology of the isostructural $Li_{2.27}K_{1.19}Zr_{2.16}O_{6.05}$ compound was determined as well. In this case, the particle size was around 1 μm. Nevertheless, the morphology of this sample was not polyhedral. In this case, particles seemed to present a flake-like morphology and their surface is less corrugated (Fig. 7).

### 3.4. $CO_2$ sorption

It has been published that $Li_2ZrO_3$, alone or doped with small quantities of potassium, presents good qualities as $CO_2$ absorbent material [5,17]. Furthermore, $Li_{2-x}Na_xZrO_3$ solid solutions present even better qualities as $CO_2$ captors than $Li_2ZrO_3$ [15,16]. Therefore, it could be expected that $Li_{2-x}K_xZrO_3$ samples present similar or better behavior as $CO_2$ captors. If $Li_{2-x}K_xZrO_3$ absorbs $CO_2$, the following reaction may occur:

$$Li_{2-x}K_xZrO_3 + CO_2 \rightarrow (Li_{2-x}K_x)CO_3 + ZrO_2, \quad (1)$$

where $(Li_{2-x}K_x)CO_3$ is simply a mixture of both alkaline carbonates, $Li_2CO_3$ and $K_2CO_3$. Fig. 8 shows the thermograms of the zirconates, which present different $CO_2$ absorption capacities, for each sample. First, $Li_2ZrO_3$ only presented a total weight increase of 2.2 wt%. Moreover, the maximum temperature of $CO_2$ sorption was 626 °C. The $CO_2$ absorption values presented by $Li_2ZrO_3$ are in good agreement with previous reports [7,9].

Then, the $Li_{1.8}K_{0.2}ZrO_3$ sample, which is the limit of solubility, presents a significant improvement in the $CO_2$ absorption. In this case, the weight increases up to 9.6 wt%, and the maximum absorption temperature practically did not present any change. It was equal to 628 °C. Besides, the absorption–desorption peak became broader than the $Li_2ZrO_3$ peak, and it seems that the $CO_2$ absorption on $Li_{1.8}K_{0.2}ZrO_3$ is faster than that of $Li_2ZrO_3$, because of the change of the slops of both curves between 500 and 600 °C.

In the third sample, $Li_{1.4}K_{0.6}ZrO_3$, the total $CO_2$ absorption was increased again (12.7 wt%). Furthermore, the curve reveals two processes. First, a loss of weight was shown between 260 and 470 °C (1.8 wt%). This loss of weight may be attributed to a deshydroxilation process or to a decomposition process of the isostructural compound, because the real composition of this sample is $Li_2ZrO_3$ (38.8%) and $Li_{2.27}K_{1.19}Zr_{2.16}O_{6.05}$ (61.2%). As none hydroxide compound was detected by XRD (see Fig. 2), it was concluded that the loss of weight corresponds to the $Li_{2.27}K_{1.19}Zr_{2.16}O_{6.05}$ decomposition. On the other hand, the second difference observed on the $Li_{1.4}K_{0.6}ZrO_3$ thermogram was a change on the maximum absorption temperature. Although the absorption process began at around the same temperature, in comparison to the other

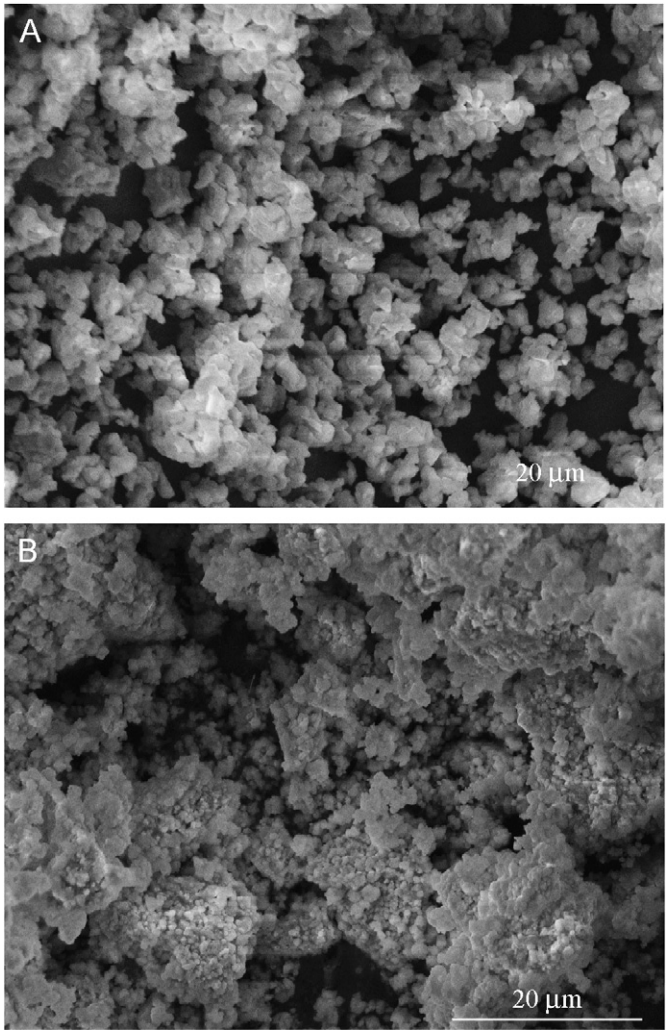


Fig. 6. SEM images of $Li_{2-x}K_xZrO_3$ samples prepared with different values of $x$. $Li_2ZrO_3$ (A) and $Li_{1.8}K_{0.2}ZrO_3$ (B).

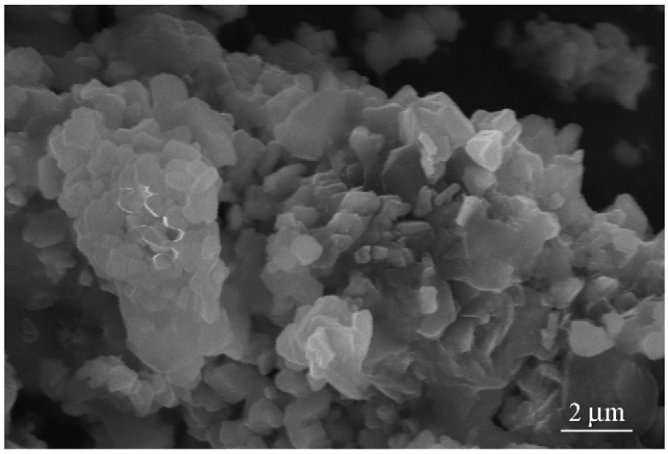


Fig. 7. SEM image of the isostructural $Li_{2.27}K_{1.19}Zr_{2.16}O_{6.05}$ phase.

two samples, the maximum absorption was reached at a higher temperature. In fact, it was shifted to 702 °C. It could be attributed, again, to the presence of $Li_{2.27}K_{1.19}Zr_{2.16}O_{6.05}$.

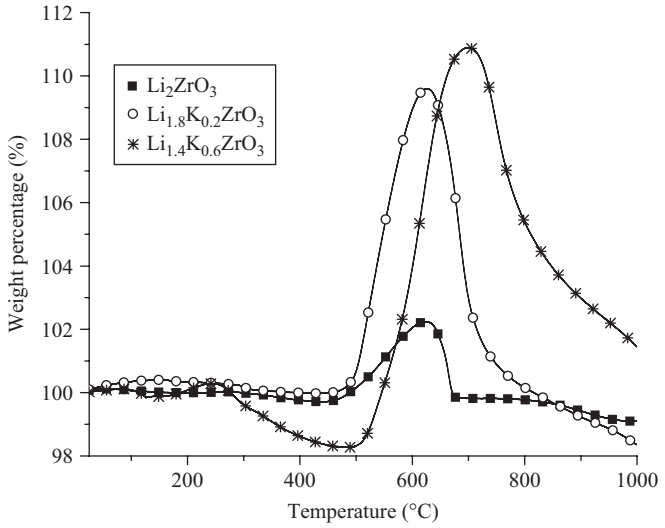


Fig. 8. Thermogravimetric analyses of $Li_2ZrO_3$, $Li_{1.8}K_{0.2}ZrO_3$ and $Li_{1.4}K_{0.6}ZrO_3$ into a flux of $CO_2$.

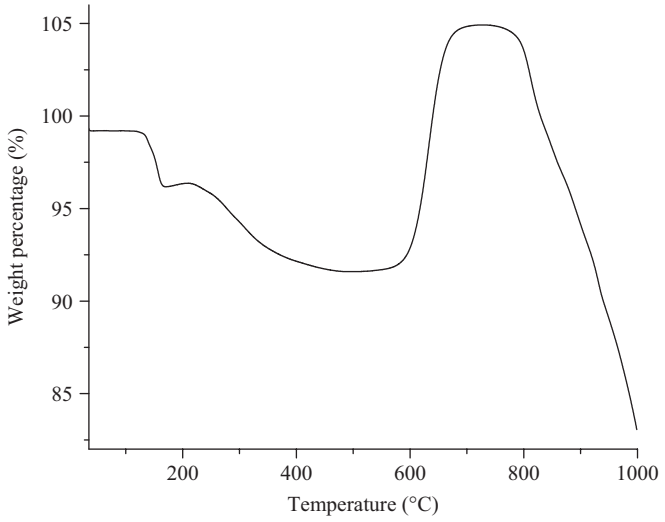


Fig. 9. Thermogravimetric analysis of the isostructural $Li_{2.27}K_{1.19}Zr_{2.16}O_{6.05}$ phase into a flux of $CO_2$.

When the same analysis was performed on the isostructural $Li_{2.27}K_{1.19}Zr_{2.16}O_{6.05}$ sample, the following results were obtained (Fig. 9). At the beginning of the thermogram, two different loss of weight were detected. First, a dehydration–deshydroxilation process was observed between 60 and 170 °C. Therefore, this sample is more hygroscopic than the other zirconates. Latter, a loss of weight from 260 to 470 °C was evidenced, as the loss of weight observed in the previous sample ($Li_{1.4}K_{0.6}ZrO_3$). This loss of weight was attributed to a partial decomposition of the compound. The total weight lost on both processes was equal to 9.4 wt%, which strongly suggests that $Li_{2.27}K_{1.19}Zr_{2.16}O_{6.05}$ is not as stable as the other samples, at least under a flux of $CO_2$. This hypothesis was confirmed at higher temperatures, where the sample loosed

more weight that that expected due to $CO_2$ desorption ($T > 800\,^{\circ}C$).

Although this compound seems not to be very stable at high temperature, its $CO_2$ sorption capacity was not negligible. The sample was able to absorb 13.3 wt%, having the maximum absorption at 728 °C. Actually, this quantity of $CO_2$ absorbed is higher that those values obtained for the other samples and the absorption temperature was shifted to higher temperatures, following the same trend.

In order to further understand the $CO_2$ caption on these ceramics some extra experiments were performed. Fig. 10 shows the isothermal graphs of $Li_2ZrO_3$, $Li_{1.8}K_{0.2}ZrO_3$ and $Li_{1.4}K_{0.6}ZrO_3$ at 550 °C. As in the thermograms (Fig. 8), $Li_{1.4}K_{0.6}ZrO_3$ lost weight at the beginning of the experiment. Therefore, the total $CO_2$ absorbed had to be adjusted. The behavior on this sample can be merely explained by the presence of $Li_{2.27}K_{1.19}Zr_{2.16}O_{6.05}$, which decomposes. Additionally, it is evident that $Li_2ZrO_3$ absorbed at slower rate than $Li_{1.8}K_{0.2}ZrO_3$ and $Li_{1.4}K_{0.6}ZrO_3$. Actually, the slopes of the curves, at short times (0–30 min), are 0.061, 0.204, and 0.306 wt% $min^{-1}$ for $Li_2ZrO_3$, $Li_{1.8}K_{0.2}ZrO_3$ and $Li_{1.4}K_{0.6}ZrO_3$, respectively. These results indicate that $Li_{1.4}K_{0.6}ZrO_3$ absorbs $CO_2$ five times faster than $Li_2ZrO_3$. However, the slopes of the three zirconates became similar at long times, due to the diffusion of lithium and potassium through the carbonate ($Li_2CO_3$ and $K_2CO_3$) external shell produced over all the surface of the particles. In the three cases, the slope of the curves only varied between 0.0089 and 0.0094 wt% $min^{-1}$. A summary of the whole $CO_2$ sorption behavior, for the three samples, is presented on Table 3. Results clearly show that potassium addition enhanced the $CO_2$ sorption.

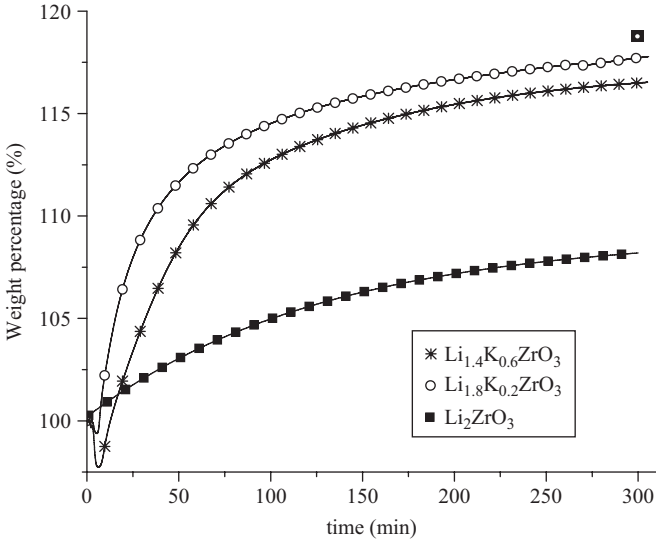


Fig. 10. Isothermal analyses of $Li_2ZrO_3$, $Li_{1.8}K_{0.2}ZrO_3$ and $Li_{1.4}K_{0.6}ZrO_3$ heat treated at 550 °C, into a flux of $CO_2$. The extra point labelled as corresponds to total $CO_2$ absorbed by $Li_{1.4}K_{0.6}ZrO_3$ after the adjusted, due to loss of weight at the beginning of the experiment.

Table 3
$CO_2$ absorption properties of the different lithium–potassium zirconates

| Sample | $CO_2$ absorbed (wt%) | Efficiency (%) | $gr_{CO2}/gr_{ceram}$ |
|---|---|---|---|
| $Li_2ZrO_3$ | 8.13 | 28.33 | 0.024 |
| $Li_{1.8}K_{0.2}ZrO_3$ | 17.7 | 64.22 | 0.177 |
| $Li_{1.4}K_{0.6}ZrO_3$ | 18.6 | 72.91[a] | 0.186[a] |

[a]Data obtained for this sample was calculated assuming the nominal formula.

$CO_2$ sorption increased as a function of the potassium added to the sample, as it was expected. Apparently, at the beginning of the absorption process, potassium induces, in some way, a higher reactivity with $CO_2$, but at long times the $CO_2$ sorption seems to become equal to the $CO_2$ sorption on the sample without potassium ($Li_2ZrO_3$). The results clearly show that $CO_2$ retention behavior cannot be explained as a sum of the corresponding retention values of the pure lithium and potassium zirconates. Therefore, structural and morphological features are as important as composition and reactivity.

This chemical behavior, observed specifically on the $Li_{2-x}K_xZrO_3$ solid solutions, may be justified with some thermodynamic data. The formation enthalpy ($\Delta H_f$) of the lithium and potassium carbonates are −1215.4 and −1151.0 kJ/mol, respectively [23,24]. As the $\Delta H_f$ of $K_2CO_3$ is 64.4 kJ/mol lower than that of $Li_2CO_3$, $Li_2CO_3$ needs more energy to be produced. In other words, at the same temperature, $K_2CO_3$ is produced faster than $Li_2CO_3$. This can explain why the reactivity is enhanced at short times with the addition of potassium. On the contrary, once $K_2CO_3$ and $Li_2CO_3$ are produced, forming a superficial shell around the ceramic particles, potassium and lithium diffusion determines the $CO_2$ sorption.

## 4. Conclusions

$Li_{2-x}K_xZrO_3$ solid solutions were prepared by the precipitation method. The limits of potassium solubility into $Li_2ZrO_3$ were determined by XRD. Additionally, during the synthesis of these solid solutions, it was found a new lithium–potassium zirconate phase, which was estimated to have the following stoichiometry: $Li_{2.27}K_{1.19}Zr_{2.16}O_{6.05}$. Previously, there was already reported the crystal structure of a similar, but more complex, compound $Li_{1.8}K_{0.9}Mg_{0.75}Zr_{2.25}O_{6.6}$. Both compounds present a very close crystal structure, existing a distortion over the *c*-axis, due to switch between the Li and Mg atoms. The positions occupied by Mg in the previous structure are now simple occupied by lithium and/or potassium atoms.

$Li_{2-x}K_xZr_2O_3$ solid solutions presented higher $CO_2$ absorption capacities, if compared to pure $Li_2ZrO_3$. The different $Li_{2-x}K_xZr_2O_3$ solid solutions absorbed $CO_2$ between 450 and 730 °C, but ceramics containing potassium absorbed $CO_2$ at higher temperatures. Even, $CO_2$

absorption of $Li_{2.27}K_{1.19}Zr_{2.16}O_{6.05}$ is better than $Li_2ZrO_3$, and as the lithium potassium zirconate solid solutions, the maximum temperature of absorption was shift to higher temperatures.

The kinetic analyses indicate that $Li_{2-x}K_xZrO_3$ solid solutions can absorb $CO_2$ up to five times faster than $Li_2ZrO_3$ at short times. Latter, at long times, the kinetic curves clearly indicate that $CO_2$ absorption of all the zirconates became similar, due to the diffusion of lithium and potassium through the carbonate ($Li_2CO_3$ and $K_2CO_3$) external shell. All this chemical behavior was explained in terms of the formation enthalpy of the lithium and potassium carbonates.

## Acknowledgments

This work was financially supported by the Mexican government through the project 23418-SEMARNAT-CONACYT and by the Universidad Nacional Autónoma de Mexico (IN103506 PAPIIT). Furthermore, authors thank to L. Baños, E. Fregoso and J. Guzman, for technical help in the XRD, thermal and SEM analyses, respectively.

## References

[1] H. Pfeiffer, P. Bosch, S. Bulbulian, J. Nucl. Mater. 257 (1998) 309–317.
[2] G.C. Lu, L. Wei-Cheng, J. Mater. Chem. 10 (2000) 1403–1407.
[3] J.M. Tarascon, M. Armand, Nature 414 (2001) 359–368.
[4] C.A. Vincent, Solid State Ionics 134 (2000) 159–167.
[5] K. Nakagawa, T. Ohashi, J. Electrochem. Soc. 145 (1998) 1344–1346.
[6] B.N. Nair, T. Yamaguchi, H. Kawamura, S.I. Nakao, K. Nakagawa, J. Am. Ceram. Soc. 87 (2004) 68–74.
[7] H. Pfeiffer, P. Bosch, Chem. Mater. 17 (2005) 1704–1710.
[8] H. Mosqueda, C. Vazquez, P. Bosch, H. Pfeiffer, Chem. Mater. 18 (2006) 2307–2310.
[9] K.H. Choi, Y. Korai, I. Mochida, Chem. Lett. 32 (2003) 924–925.
[10] R. Xiong, J.I. Ida, Y.S. Lin, Chem. Eng. Sci. 58 (2003) 4377–4385.
[11] S.K. Wirawan, D. Creaser, Microporous Mesoporous Mater. 91 (2006) 196–205.
[12] A. Macario, A. Katovic, G. Giordano, F. Iucolano, D. Caputo, Microporous Mesoporous Mater. 81 (2005) 139–147.
[13] K. Nombra, K. Tokumistu, T. Hayakawa, Z. Homonnay, J. Radioanal. Nucl. Chem. 246 (2000) 69–77.
[14] Z. Yong, A.E. Rodrigues, Energy Convers. Manage. 43 (2002) 1865–1876.
[15] H. Pfeiffer, E. Lima, P. Bosch, Chem. Mater. 18 (2006) 2642–2647.
[16] H. Pfeiffer, C. Vazquez, V.H. Lara, P. Bosch, Chem. Mater. 419 (2007) 922–926.
[17] J.I. Ida, R. Xiong, Y.S. Lin, Sep. Purif. Technol. 36 (2004) 41–51.
[18] G.C. Mather, R.A. Howie, B. Thiebaut, E.E. Lachowshi, D. Eadon, T. Hyde, A.R. West, J. Mater. Chem. 6 (1996) 1379–1383.
[19] J. Rodriguez-Carvajal, Computer Program FullProf, version 3.51, Laboratoire Leon Brillouin CEA, CNRS, Grenoble, France, 1998.
[20] S. Dash, D.D. Sood, R. Prasad, J. Nucl. Mater. 228 (1996) 83–116.
[21] H. Pfeiffer, K.M. Knowles, J. Eur. Ceram. Soc. 24 (2004) 2433–2443.
[22] J.E. Huheey, Inorganic Chemistry, second ed, Harla, Mexico City, Mexico, 1981.
[23] R.C. Weast, M.J. Astle (Eds.), CRC Handbook of Chemistry and Physics, 74th ed, CRC Press, Boca Raton, FL, 1993.
[24] M. Binnewies, E. Milke, Thermochemical Data of Elements and Compounds, second ed, Wiley, Weinheim, 2002.